

Dark Matter-Wave Solitons in Optical Lattices

Pearl J.Y. Louis, Elena A. Ostrovskaya, and Yuri S. Kivshar

ARC Centre for Quantum-Atom Optics and Nonlinear Physics Group, Research School of Physical Sciences and Engineering, The Australian National University, Canberra ACT 0200, Australia

Abstract. We analyze the Floquet-Bloch matter-wave spectrum of Bose-Einstein condensates loaded into single-periodic optical lattices and double-periodic superlattices. In the framework of the Gross-Pitaevskii equation, we describe the structure and analyze the mobility properties of dark matter-wave solitons residing on the background of extended nonlinear Bloch-type states. We demonstrate that interaction between dark solitons can be effectively controlled in optical superlattices.

PACS numbers: 03.75.Lm

Submitted to: *J. Opt. B: Quantum Semiclass. Opt.* ; *Topical Issue: Optical Solitons*

1. Introduction

Bose-Einstein condensates (BECs) loaded into optical lattices show a wide range of interesting physical properties and complex nonlinear dynamics. Optical lattices can be employed to study many important physical phenomena of atomic and solid state physics. The properties of coherent macroscopic matter waves in a lattice, such as the Bloch-band structure [1], macroscopic interference effects [2], Bloch oscillations and Landau-Zener tunnelling [3], have been explored in a number of experiments.

One of the many advantages in using a macroscopic quantum periodic system, such as BECs in optical lattices is that the effective periodic potential created by a standing light wave can be easily and precisely manipulated by changing the intensities, polarizations, geometry or frequencies of the interfering laser beams. For example, the depths of the periodic potential wells induced by an optical lattice can be controlled by tuning the intensities of the laser beams. The shape of the potential can also be varied by creating an optical superlattice with more than one order of periodicity. The novel possibilities for band-gap engineering offered by superlattices have been shown to lead to a variety of phase transitions in the condensate [4], and can be effectively employed for ultracold atom manipulations, such as patterned loading of atoms into lattice sites [5]. Most remarkably, periodicity of the optical lattice potential leads to the effective dispersion of the BEC wavepackets being a function of the band structure. Thus by

inducing the motion of the lattice relative to the BEC (i.e. via non-zero detuning of the laser beams), one can manage the dispersion properties of a matter wave [6, 7].

Coherent matter waves are inherently nonlinear due to the presence of interatomic interactions. One of the common features of nonlinear dispersive systems is the existence of solitons. *Bright solitons* are localized wavepackets where the effects of dispersion are balanced by nonlinearity to produce self-trapping. In Bose-Einstein condensates, bright solitons require very special conditions to be observed. Without a periodic potential, an attractive nonlinearity and a low number of atoms within each soliton (to prevent condensate collapse) is required [8, 9]. In an optical lattice, bright matter-wave solitons have been predicted to exist, due to the balance of repulsive atomic interactions and negative effective dispersion near a band edge [11, 12, 13, 14, 15, 16, 17, 18]. Bright solitons of repulsive BEC take the form of *gap solitons*, embedded in the spectral gaps of the linear Bloch-wave spectrum.

In the majority of condensates currently created experimentally, the interatomic interaction is repulsive. This corresponds to an effectively defocusing nonlinearity of the matter-wave which can support *dark solitons* - localized dips on the condensate density background with a phase gradient across the localized region. Similar to other types of solitons, they can remain dynamically stable due to the balancing effects of nonlinearity and the (positive) dispersion. Dark solitons have been created experimentally in repulsive condensates by using a phase-imprinting technique to apply a sharp phase gradient to a condensate cloud in a magnetic trap [19, 20]. In the case of BECs loaded into optical lattices, i.e. with the possibility for dispersion management, dark solitons can be supported in both repulsive (for positive effective dispersion) and attractive condensates (for negative effective dispersion). Moreover, dark lattice solitons are expected to be easier to create experimentally than bright gap solitons, as they are not confined to the spectral gaps [21], and a phase-imprinting technique can be applied to a nonlinear Bloch-wave background within a spectral band. Alternatively, trains of dark solitons can be created in a periodic potential via Bragg scattering [22].

The theory of dark solitons has been developed extensively for many types of periodic systems such as discrete atomic chains and waveguide arrays [23, 24, 25, 26, 27]. Applying the concepts of discrete dynamical systems to the physics of the Bose-Einstein condensates in optical lattices, Abdullaev *et al.* [28] studied dark and bright solitons on non-zero backgrounds in a vertical lattice by employing a discrete mean-field model derived in the tight-binding approximation, i.e. considering a single isolated band of the Bloch-wave spectrum. In contrast, Yulin and Skryabin [21] used a single-gap continuous coupled-mode model in order to examine the stability and existence of out-of-gap dark and bright solitons. A more general analysis based on the continuous Gross-Pitaevskii equation with a periodic potential was presented by Alfimov *et al.* [29] who showed that for a repulsive condensate in an optical lattice, dark solitons can exist as stationary localized solutions with nonvanishing asymptotics. Alfimov *et al.* [29] as well as Konotop and Salerno [13] also found numerically stable dark solitons for periodic quasi-one-dimensional BEC systems. The weak spectral instability of the dark solitons in the

combined optical lattice and a strong harmonic potential, both in the discrete and continuous mean-field models, has been established in [30].

In this paper we study the structure and mobility properties of dark solitons in single and double-periodic optical lattices (superlattices) by employing the full continuous mean-field model. First, we describe the multiple band structure of the condensate Bloch-wave spectrum and analyze the Bloch waves corresponding to the band edges of the matter-wave spectrum of a single-periodic optical lattice. We then extend this analysis to the case of a double-periodic optical superlattice and demonstrate that extra mini-gaps appear in the matter-wave spectrum. We show that in-band Bloch states can support dark solitons, and find numerically continuous families of dark solitons imprinted onto the nonlinear Bloch waves of a repulsive BEC. These localized states display some properties found in discrete lattice models, including the existence of the pinning (Peierls-Nabarro) potential [31] that inhibits the solitons mobility and interactions even in the shallow-well case. Pairs of dark solitons with opposing phase gradients always experience a repulsive interaction in the lattice-free case [33], and we show that an optical superlattice can be used to initiate and effectively control the interactions of dark lattice solitons.

2. Model

The dynamics of a Bose-Einstein condensate loaded into an optical lattice can be described in the mean field approximation, by the Gross-Pitaevskii (GP) equation for the macroscopic condensate wavefunction $\Psi(x, r, t)$,

$$i\hbar \frac{\partial \Psi}{\partial t} = \left\{ -\frac{\hbar^2}{2m} \nabla^2 + V(x, r) + g_{3D} |\Psi|^2 \right\} \Psi \quad (1)$$

where $r = (y, z)$, $V(x, r)$ is the time-independent trapping potential, and $g_{3D} = 4\pi\hbar^2 a_s / m$ characterizes the two-body interactions for a condensate with atoms of mass m and s-wave scattering length a_s . The scattering length a_s is positive for repulsive interactions and negative for attractive interactions. For the cases examined in this paper, we use the parameters set by ^{87}Rb : $m = 1.44 \times 10^{-25}$ kg and $a_s = 5.7$ nm.

We consider a trapping potential $V(x, r)$ of the form

$$V(x, r) = \frac{1}{2} m \omega_{\perp}^2 (x^2 + \Omega^2 r^2) + V_L(x), \quad (2)$$

where $r^2 = y^2 + z^2$, and $\Omega = \omega_{\perp} / \omega_x$. The first term of the potential describes an anisotropic parabolic potential due to a magnetic trap, and $V_L(x)$ is the effective periodic potential formed by a quasi-1D optical lattice of the form,

$$V_L(x) = U [\varepsilon \sin^2(K_1 x) + (1 - \varepsilon) \sin^2(K_2 x)], \quad (3)$$

where $0 \leq \varepsilon \leq 1$. The superlattice potential given by Eq. (3) can be obtained by creating two separate far-detuned quasi-1D single-periodic lattices using lasers of different wavelengths, e.g. $\lambda_1 > \lambda_2$. If the two lattices are orthogonally polarized, when they are superimposed, the resulting dipole trapping potential is proportional to the sum

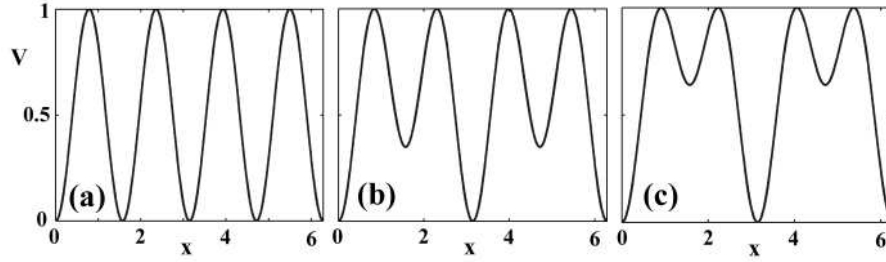


Figure 1. The structure of the superlattice potential described by Eq. (5) for different values of ε and a fixed potential height $V_0 = 1$. (a) Single-periodic optical lattice for $\varepsilon = 0$, (b,c) double-periodic superlattice with the height and periodicity unchanged, for (b) $\varepsilon = 0.3$ and (c) $\varepsilon = 0.5$, respectively.

of their individual intensities. With this interpretation, U is proportional to the total intensity and ε related to the relative intensities of the two standing light waves. The lattice wavevectors are $K_1 = 2\pi/\lambda_1$ and $K_2 = 2\pi/\lambda_2$, and the larger of the two periods is $d = \lambda_1/2$. In this paper we choose $\lambda_1/\lambda_2 = 2$ (e.g. $\lambda_1 = 700$ nm and $\lambda_2 = 350$ nm)

Eq. (1) can be made dimensionless using the characteristic length $a_L = d/\pi$, energy $E_{rec} = \hbar^2/ma_L^2$, and time $\omega_L^{-1} = \hbar/E_{rec}$ scales of the lattice. In dimensionless units, the two-body interaction coefficient is given by $g_{3D} = 4\pi(a_s/a_L)$, and the lattice depth is measured in units of the lattice recoil energy, E_{rec} . Furthermore, assuming that the condensate cloud is strongly elongated in x -direction ($\Omega > 10^{-1}$), the system can be considered to be quasi-1D. The condensate wavefunction is then separable $\Psi(x, r, t) = \Phi(r)\psi(x, t)$, with $\Phi(r)$ well described by the ground-state of a two-dimensional radially symmetric quantum harmonic oscillator, with the normalization $\int_{-\infty}^{\infty} |\Phi|^2 dy dz = 1$. Integrating dimensionless Eq. (1) over the transverse co-ordinates, gives the 1D GP equation:

$$i\frac{\partial\psi}{\partial t} = \left\{ -\frac{1}{2}\frac{\partial^2}{\partial x^2} + V(x) + g_{1D}|\psi(x, t)|^2 \right\} \psi \quad (4)$$

where $g_{1D} = 8(a_s/a_L)(\omega_L/\omega_{\perp})^2$. As the magnetic confinement along the axial direction is weak, we can ignore its contribution to $V(x)$ so that the external potential is approximated by the quasi-1D periodic potential of the optical lattice along the direction of weak confinement:

$$V(x) = V_L(x) = U[\varepsilon \sin^2(x) + (1 - \varepsilon) \sin^2(2x)], \quad (5)$$

where the amplitudes U and ε are experimentally controlled parameters and can be varied in our model. The shape of an optical superlattice depends on the values of these parameters. In the limits $\varepsilon \rightarrow 0, 1$, the lattice becomes single-periodic, and U is equal to the height of the lattice V_0 . For $\varepsilon \neq 0, 1$, Eq.(5) describes a double-periodic superlattice, with the lattice amplitude, U , defined through the height of the periodic potential, V_0 ,

as

$$U = 16V_0 \frac{1 - \varepsilon}{(4 - 3\varepsilon)^2}$$

Figure 1 shows that the superlattice potential consists of a series of alternating small and large wells. As seen in the figure, by changing the intensities of the two component standing waves (i.e. varying ε), the relative depth of lattice wells can be manipulated whilst keeping the height, V_0 , and the periodicity of the lattice constant.

3. The matter-wave band-gap spectrum

The stationary states of a condensate in a quasi-1D infinite periodic potential are described by solutions of Eq. (4) of the form: $\psi(x, t) = \phi(x) \exp(-i\mu t)$, where μ is the corresponding chemical potential. The steady-state wave function $\phi(x)$ obeys the time-independent GP equation

$$\left[\frac{1}{2} \frac{d^2}{dx^2} - V(x) + \mu - g_{1D} |\phi(x)|^2 \right] \phi(x) = 0, \quad (6)$$

where $V(x)$ is defined in Eq. (5).

The case of a noninteracting condensate formally corresponds to $g_{1D} = 0$. Eq. (6) is then linear in ϕ and the condensate wave function can be presented as a superposition of Bloch waves,

$$\phi(x) = b_1 \phi_1(x) e^{ikx} + b_2 \phi_2(x) e^{-ikx}, \quad (7)$$

where $\phi_{1,2}(x)$ have periodicity of the lattice potential, $b_{1,2}$ are constants, and k is the Floquet exponent. The linear matter-wave spectrum consists of bands of eigenvalues $\mu_{n,k}$ in which $k(\mu)$ is a real wavenumber of amplitude-bounded oscillatory Bloch waves. The bands are separated by “gaps” in which $Im(k) \neq 0$. The solutions at the band edges are exactly periodic stationary Bloch states. For an interacting condensate ($g_{1D} \neq 0$), bright *gap* soliton solutions exist for the chemical potentials corresponding to the gaps of the linear matter-wave spectrum [11, 12, 13, 14, 15, 16, 17, 18].

Figure 2 presents the band-gap diagram on the plane (μ, V_0) for the Bloch-wave solutions of Eq. (6) for the case of a noninteracting condensate in the lattice described by Eq. (5) for different lattice parameters. Only the lowest energy transmission bands are shown. The band-gap structure of a single-periodic optical lattice ($\varepsilon = 0$, shaded) is compared with that of a double-periodic lattice or superlattice ($\varepsilon = 0.05$, dashed curves). The mini-gaps the superlattice opens up ‘inside’ the transmission band regions of the single-periodic lattice are clearly visible. As $\varepsilon = 0.05$ is close to $\varepsilon = 0$, there is significant overlap between the two linear band-gap spectra. However, as $\varepsilon \rightarrow 1$, the two spectra diverge. Fig. 2(b) shows the spatial structure of the Bloch wave solutions, $\phi_{\text{Lin}}(x)$ at the edges of the single-periodic transmission bands for a lattice height of $V_0 = 1$. Dotted lines show the potential and ϕ_{Lin} is normalized according to the condition, $\int_0^\pi |\phi_{\text{Lin}}|^2 dx = \pi$.

Figure 3(a) shows the band-gap structure for a noninteracting condensate in a superlattice with $\varepsilon = 0.3$ compared to that of a single-periodic lattice, both for a

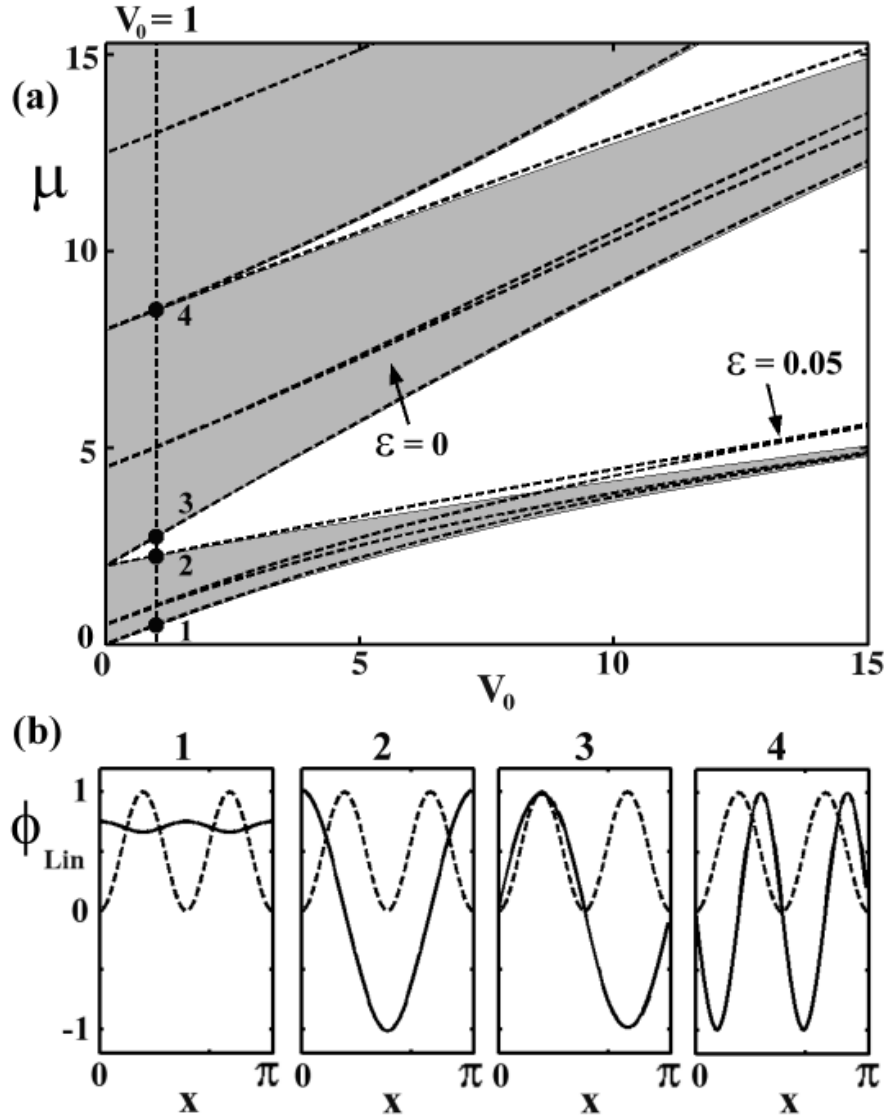


Figure 2. (a) The matter-wave band-gap spectrum of Bloch waves in the linear regime (noninteracting condensate). The shaded areas show the lowest bands of Bloch matter-waves in a single-periodic lattice ($\varepsilon = 0$). The solid lines mark the band edges corresponding to periodic Bloch states, examples of which are shown in (b) for a lattice of the height $V_0 = 1$. The band edges of the matter-wave spectrum for a superlattice at $\varepsilon = 0.05$ are shown by the dashed curves.

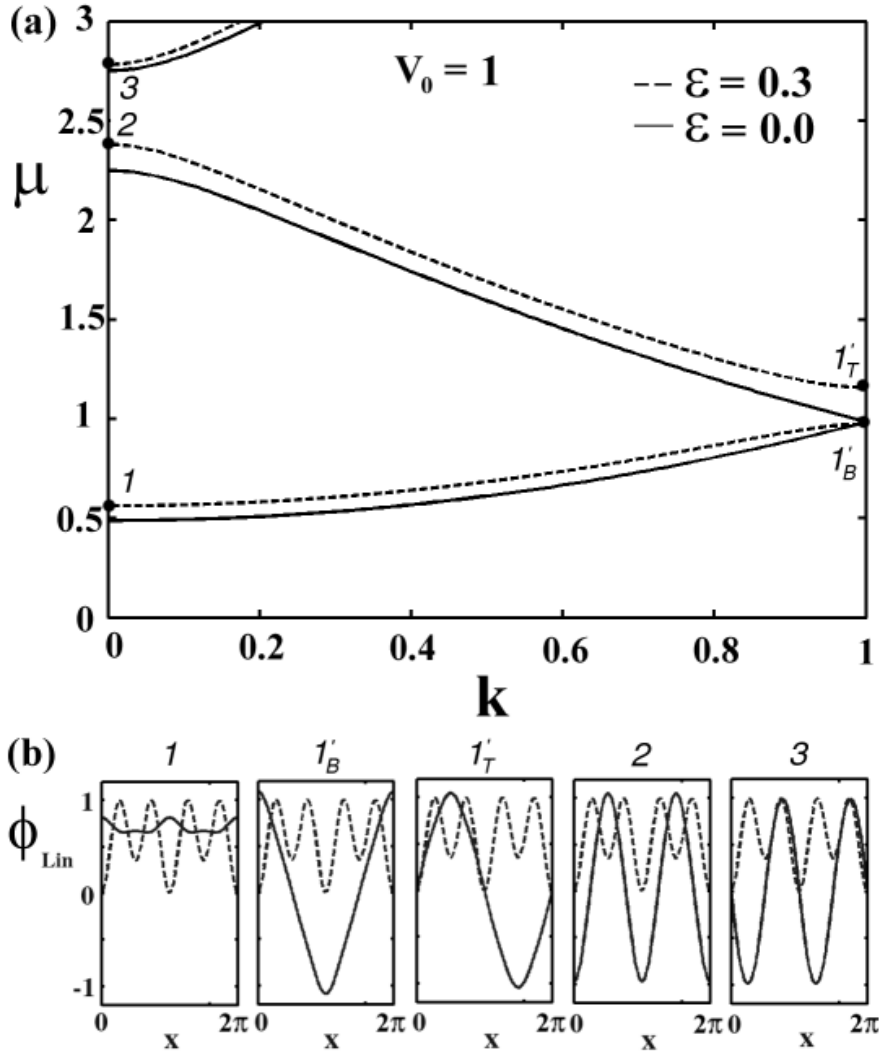


Figure 3. (a) The band-gap spectrum for a noninteracting BEC in a superlattice (dotted lines: $\varepsilon = 0.3$) compared to that of a single-periodic lattice (solid lines: $\varepsilon = 0$), both at $V_0 = 1$. (b) The spatial structure of periodic Bloch-wave solutions at the edges of the superlattice bands for $\varepsilon = 0.3$ and $V_0 = 1$

lattice height of $V_0 = 1$. The bands of the single-periodic lattice are ‘folded back’ into the first Brillouin zone ($0 \leq k \leq 1$) of the superlattice. The edges of the first mini-gap ($1'_B$, $1'_T$) are clearly visible. Fig. 3(b) shows examples of the structure of the periodic Bloch waves at the edges of the superlattice transmission bands. The dotted lines show the superlattice potential and ϕ_{Lin} is normalized according to the condition, $\int_0^{2\pi} |\phi_{Lin}|^2 dx = \pi$. With the small wells breaking the symmetry of the sinusoidal potential, Bloch wave solutions exist with peaks in the small wells and/or the large wells of the superlattice. The periodic Bloch waves at band-edges 1 , $1'_B$, $1'_T$ and 2 have discrete counterparts in the solutions of the well-known diatomic lattice

problem. The extended solutions in higher-order bands cannot be described using the standard single-band discrete approximation.

4. Dark solitons

4.1. Single-periodic lattices

We find different families of dark soliton solutions by using a standard relaxation technique to numerically solve Eq. (6) for a lattice potential $V(x)$ given by Eq. (5). In this subsection we describe our results for the single-periodic case ($\varepsilon = 0$). In the following subsections we will expand our investigations to the more complicated double-periodic superlattice. Although we only study dark solitons associated with the lowest bands of the matter-wave spectrum, our results should qualitatively apply to dark solitons of the higher order bands.

Figures 4(a,b) show the families of dark solitons for a single-periodic optical lattice of height $V_0 = 1$. According to Figure 2, this is in the shallow well regime, where the bands are broad, the condensate behaves like a superfluid, and the coupling between lattice wells is strong. Figure 4(a) plots the complementary power, P_c of the dark soliton families against the chemical potential μ . P_c is defined as follows,

$$P_c = \int \left[\phi_{\text{Background}}^2(x) - \phi_{\text{Soliton}}^2(x) \right] dx \quad (8)$$

The complementary power characterizes a deficit of the condensate atoms associated with the formation of a dark-soliton notch in the Bloch wave background.

By analogy with bright spatially localized states of the condensate in a lattice, there exist two distinct types of dark solitons - those centered on the minimum (on-site) and maximum (off-site) of the lattice potential. The families of the on-site and off-site dark solitons, characterized by the dependence $P_c(\mu)$, are plotted in Figure 4(a). The two families of dark solitons originate at the bottom edge of each band of the linear matter-wave spectrum. The splitting of the power between the families becomes prominent for large μ in the first band, but is negligible for the families originating in the second band. As can be seen in Figure 4(b), each of these dark solitons rests on a periodic matter-wave background. Near the bottom edge of a band, the background has a spatial structure of a linear periodic Bloch wave at the corresponding band edge [cf. Fig 2(b)]. For larger μ , when the linear theory becomes invalid, the background mode describes a *nonlinear* Bloch wave, which is a periodic solution of the nonlinear time-independent Gross-Pitaevskii equation [15]. The effect of the interatomic interactions (i.e. nonlinearity) is to cause an effective shift of the band edges. Therefore the nonlinear Bloch waves can be found in spectral regions beyond the linear bands. Correspondingly, the families of dark solitons originate within but extend well beyond the band.

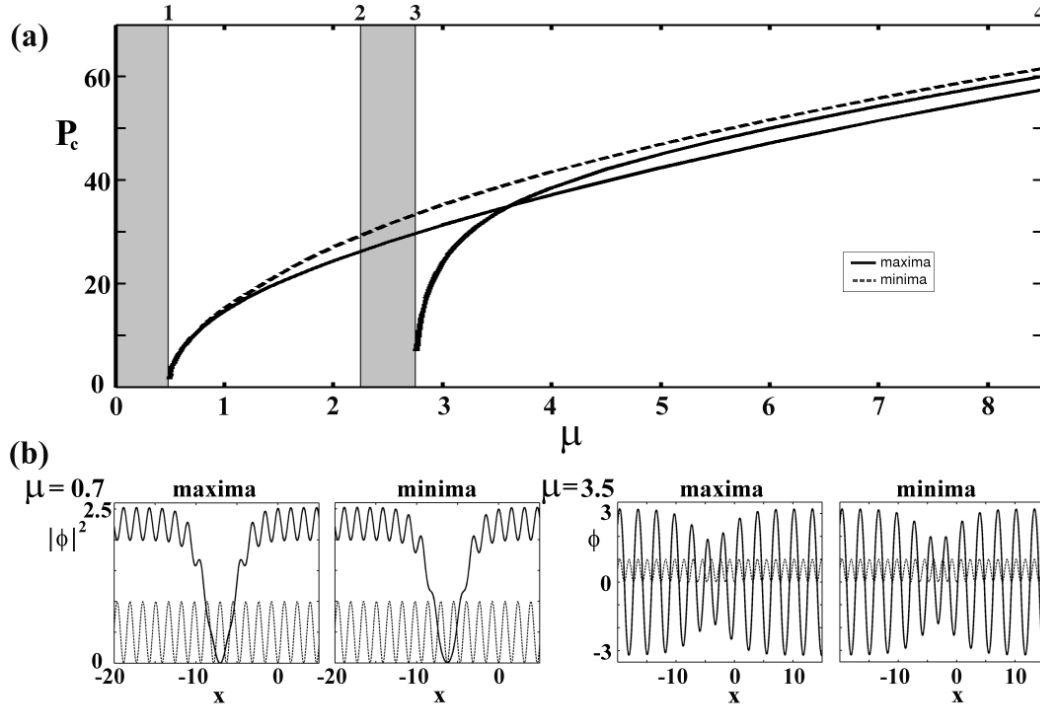


Figure 4. (a) The complementary powers P_c of families of the on-site (solid) and off-site (dashed) dark solitons in a single-periodic lattice ($\varepsilon = 0$) for $V_0 = 1$. Shaded - gaps of the linear matter-wave spectrum. Unshaded - bands, with the band edges numbered. (b) Examples of the spatial structure of the dark soliton families shown in (a).

4.2. Superlattices

In the previous subsection, we examined the limiting case of $\varepsilon = 0$ corresponding to a single-periodic lattice. Here we study the dark solitons in a superlattice, where $0 < \varepsilon < 1$ and a second periodicity is introduced to the system, as shown in Figure 1 above. As shown in Section 3, the addition of the extra periodicity to the lattice potential causes large structural changes in the matter-wave band-gap spectrum as well as the spatial structure of the Bloch states (and hence to the nonlinear Bloch waves). Dark solitons can now appear at the edges of the mini-gaps opened by the superlattice.

We found dark soliton solutions to Eq. (6) for a superlattice potential with $\varepsilon = 0.3$ and a lattice height of $V_0 = 1$ (shallow well regime) numerically. For this superlattice potential, the minigaps are inside the bands of the matter-wave spectrum of the single-periodic lattice. Figure 5(a) shows the complementary powers of the dark solitons in the two bands around the first mini-gap opened by the superlattice potential. The two families in each band correspond to the dark states centered on a large or a small lattice well. The latter state transforms into an off-site dark soliton in the limit $\varepsilon \rightarrow 1$, and into an on-site soliton in the limit $\varepsilon \rightarrow 0$. Figure 5(b) presents examples of the

spatial structure of each of the dark soliton families. As in the case of dark solitons in a single-periodic lattice, the dark solitons in a superlattice describe kink-like modes on a non-zero background that, away from the soliton, becomes a nonlinear Bloch wave. The families of dark solitons originate at the bottom edges of the linear bands and extend beyond the bands as nonlinearity grows.

As μ is increased, the power splitting between two families becomes prominent in each of the two bands shown in Figure 5(a). In the single-periodic case, the dark solitons centered at a potential minimum always had lower complementary powers than the family centered at the potential maximum. A superlattice allows us to have dark solitons centered in wells of different levels of trapping and as can be seen Figure 5(a) the more ‘stable’ family seems to alternate between dark solitons centered at a large well and those centered at a small well. Similar power splitting behaviour has been observed for bright gap solitons in binary waveguide arrays recently analyzed in [32]; for that model the power splitting can be connected to alternating stability properties.

Stability is a large and as yet unexplored question for dark matter-wave solitons in optical lattices. Several analytical techniques have been developed to study stability of dark solitons and are outlined in a review paper by Kivshar and Luther-Davies [33]. However, a rigorous analysis of stability of dark matter-wave solitons in an optical lattice is complicated by the fact that their backgrounds are not constant but take the form of nonlinear Bloch waves. These have their own stability properties which have been explored in [34, 13]. These studies suggest that only the ground state nonlinear Bloch wave can be modulationally stable. Some work on the stability of dark matter-wave solitons in optical lattices have been conducted by Yulin and Skryabin, in the framework of a coupled-mode model [21]. Yulin and Skryabin found that whilst bright out-of-gap solitons on a bright background are unstable, the stability of dark out-of-gap solitons depends on the stability of the background [21]. The study of stability of dark solitons in optical superlattices in the framework of the full mean-field model is beyond the scope of the present paper.

4.3. Soliton interactions

The difference in the complementary powers of the soliton families described above can be associated with the difference between the minimal values of the energy functional,

$$E = \int \left[\frac{1}{2}(\nabla\phi)^2 + V_L(x)\phi^2 + \frac{1}{2}g_{1D}\phi^4 \right] dx,$$

for the two different types of the stationary dark solitons. This energy difference corresponds to the maximum of an effective potential of the lattice known as the Peierls-Nabarro (PN) potential [31]. The height of the PN potential can be understood as the minimum energy required to move a localized wavepacket by one lattice site, i.e. the difference between the energies of a soliton located at a minimum of the periodic lattice and one at a maximum. As was shown for bright localized modes in a discrete lattice, the two different stationary states can be seen to represent a moving mode at different

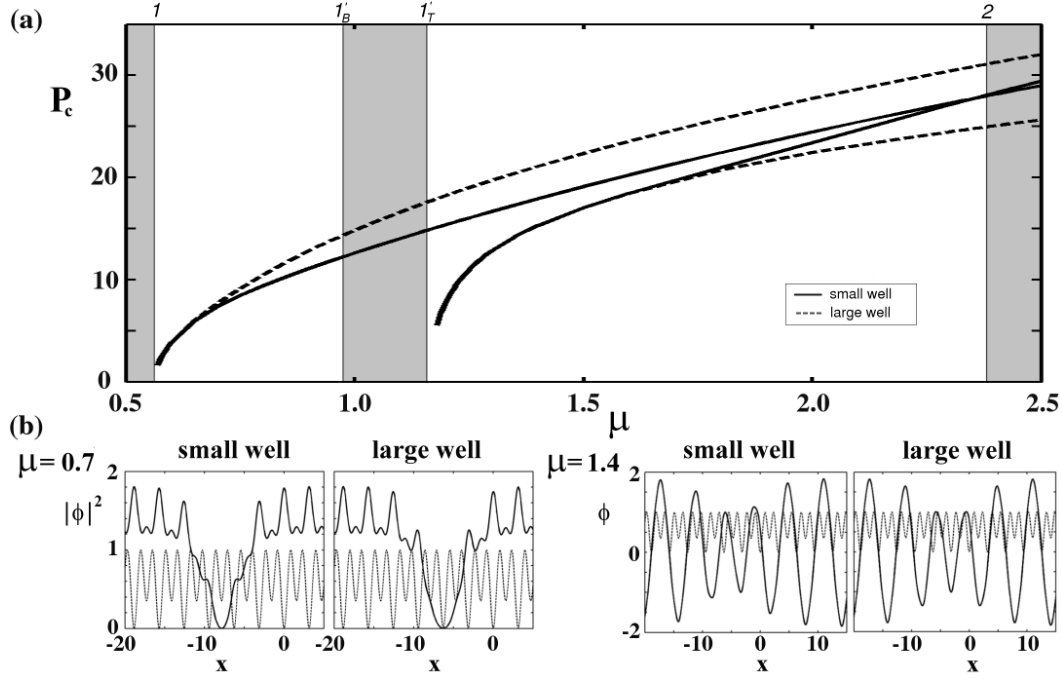


Figure 5. (a) The complementary powers P_c of two families of dark solitons in a superlattice ($\varepsilon = 0.3$) with $V_0 = 1$. Shaded areas show the gap regions of the linear matter-wave spectrum. Unshaded areas show the transmission bands with the band edges numbered. The two bands shown here surround the first mini-gap (gap edges $1'_B$ and $1'_T$). (b) Examples of the spatial structure of the dark soliton families in (a).

times, therefore the knowledge of the PN potential height is essential in answering the questions about possible mobility of a lattice soliton and its ability to interact with other localized states [31].

Analytical and numerical calculations of the PN potential for the bright gap solitons have recently been performed in the discrete GP model [35], assuming the tight-binding regime of the BEC dynamics. Remarkably, it has been established that the tight binding calculations of the PN potential fail to match the results for the full continuous model even in the regime of parameters where the approximation is well justified. Here, we calculate the PN potential height for the two types of dark solitons found both in the single- and double-periodic lattice, and show the results of the calculations for different values of μ in Fig. 6. In a single-periodic lattice [Fig. 6 (a)], for the moderate values of μ within the first band, the dependence has a "flat" region followed by a region where the PN barrier for the on-site dark soliton is positive. Therefore the dark on-site soliton is effectively pinned by the lattice. For the superlattice, the steep positive region of the PN barrier height near the first band edge [Fig. 6 (b)] indicates that the motion and interaction of the solitons could be easily initiated, if initially the dark state is centered on a *small well* of the superlattice potential. The inflection of the dependence at larger μ could indicate that, for the shallow lattice, the nonlinear effects

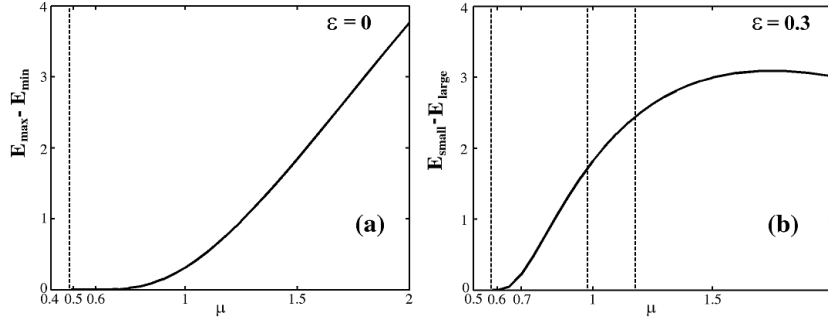


Figure 6. PN potential height shown a difference in soliton energies vs. chemical potential for (a) a single-periodic lattice and (b) a superlattice of the same height $V_0 = 1$. Vertical dashed lines - the band edges.

on the soliton dynamics become more important than those due to the lattice potential. Clearly, for a fixed chemical potential, lattice height, and periodicity, variation of the superlattice parameter ϵ controls the height of the PN potential and therefore mobility and interaction properties of the dark solitons.

To model interactions between dark matter-wave solitons in an optical lattice we integrate Eq. (4) using a pseudo-spectral Fourth Order Runge-Kutta method in the interaction picture. The code is implemented using the **xmds** code generator [36]. We study interaction between dark solitons in the framework of two models of optical lattice potentials described above, i.e. (i) a single-periodic lattice with $\epsilon = 0$ and (ii) an optical superlattice with $\epsilon = 0.3$. In each case, the lattice height is fixed to $V_0 = 1$. The initial conditions for both lattices are a pair of dark solitons on a ground-state nonlinear Bloch wave background [see Figs. 4(b) and 5(b)]. The chemical potential is slightly different in each case so as to have the same maximum density (and hence nonlinearity) for both lattices. The initial spatial separation between the dark solitons in a pair is 6π . For the superlattice this corresponds to a spatial separation of 6 wells. For the single-periodic lattice, a spatial separation of 12 wells. The results of the temporal dynamics are shown in Figure 7 (for the values of μ near the bottom edge of the first band), and seem to agree with the qualitative predictions from the PN calculations.

Figure 7(a) shows that even in the shallow-well regime, a single-periodic potential is sufficient to trap the dark solitons due to the effect of the large positive PN potential height (both solitons are initially centered at the potential minima). In this case, the density perturbation of the matter wave develops from the numerical noise. By adding the amplitude perturbation to the initial conditions, one can observe damped oscillations of the individual soliton positions around the potential minimum (not shown). In the superlattice potential, if both solitons are initially centered at the large wells of the lattice potential, the dark solitons are also trapped by the lattice, as in Figure 7(b). However, if the solitons are shifted so that they are initially centered at the small wells of the lattice potential they are able to move and repel each other, as shown in Figure 7(c).

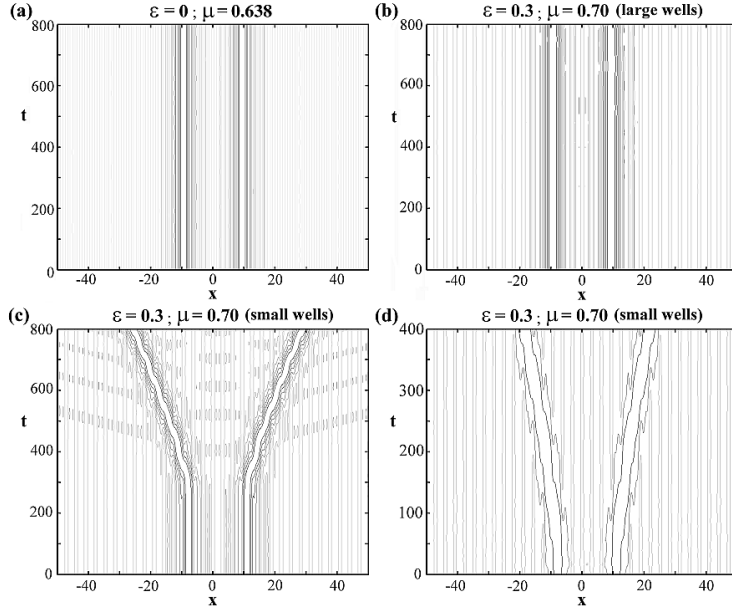


Figure 7. Control of the dark soliton interactions in optical lattices. Shown is the contour plot of the condensate density in the interaction region as a function of time ($V_0 = 1$). Initially, a pair of dark solitons on a nonlinear Bloch wave background is centered in (a) the wells of a single-periodic lattice, (b) the large wells of a superlattice, and (c) the small wells of a superlattice. In (d) symmetric amplitude and phase perturbation is added to the initial condition of (c) at $t = 0$.

The addition of amplitude perturbations to the initial state almost immediately triggers a rapid soliton separation Figure 7(c). The same effect can be achieved by changing the contrast of the superlattice by increasing ε whilst keeping the periodicity and lattice height constant.

5. Conclusions

We have analyzed the band-gap structure of the Floquet-Bloch matter waves in optical lattices and superlattices in the framework of the Gross-Pitaevskii equation with a single- and double-periodic potential. We have shown that each type of the nonlinear Bloch matter-waves can support dark solitons - localized, stationary notches in the condensate background density with a phase gradient. We have described different families of dark solitons originating within the multiple bands of the Floquet-Bloch matter wave spectrum. By considering the continuous analogue of the Peierls-Nabarro potential in discrete lattices, we have demonstrated that the mobility and interaction properties of the dark solitons can be effectively controlled by changing the structure of an optical superlattice.

Acknowledgments

The authors acknowledge a support from the Australian Research Council and useful discussions with Dr. Craig Savage.

References

- [1] Denschlag J H, Simsarian J E, Häffner H, McKenzie C, Brownnaeys A, Cho D, Helmerson K, Rolston S L and Phillips W D 2002 *J. Phys. B* **35** 3095
- [2] Anderson B P and Kasevich M A 1998 *Science* **282** 1686
- [3] Cristiani M, Morsch O, Müller J H, Ciampini D and Arimondo E 2002 *Phys. Rev. A* **65** 063612
- [4] Roth R and Burnett K 2003 *J. Opt. B* **5** S50
- [5] Peil S, Porto J V, Tolra B L, Obrecht J M, King B E, Subbotin M, Rolston S L and Phillips W D 2003 *Phys. Rev. A* **67** 051603
- [6] Eiermann B, Treutlein P, Anker Th, Albiez M, Taglieber M, Marzlin K-P and Oberthaler M K 2003 *Phys. Rev. Lett.* **91** 060402
- [7] Fallani L, Cataliotti F S, Catani J, Fort C, Modugno M, Zawada M and Inguscio M 2003 arXiv:cond-mat/0303626
- [8] Strecker K E *et al.* 2002 *Nature* (London) **417**, 150
- [9] Khaykovich L *et al.*, 2002 *Science* **296**, 97
- [10] Orzel C, Tuchman A K, Fenselau M L, Yasuda M and Kasevich M A 2001 *Science* **291** 2386
- [11] Zobay O, Pötting S, Meystre P and Wright E M 1999 *Phys. Rev. A* **59** 643
- [12] Trombettoni A and Smerzi A 2001 *Phys. Rev. Lett.* **86** 2353
- [13] Konotop V V and Salerno M 2002 *Phys. Rev. A* **65** 021602
- [14] Hilligsøe K M, Oberthaler M K and Marzlin K-P 2002 *Phys. Rev. A* **66** 063605
- [15] Louis P J Y, Ostrovskaya E A, Savage C M and Kivshar Y S 2003 *Phys. Rev. A* **67** 013602
- [16] Ostrovskaya E A and Kivshar Y S 2003 *Phys. Rev. Lett.* **90** 160407
- [17] Carusotto I, Embriaco D and Giuseppe C L R 2002 *Phys. Rev. A* **65** 053611
- [18] Efremidis N K and Christodoulides D N 2003 *Phys. Rev. A* **67** 063608
- [19] Burger S, Bongs K, Dettmer S, Ertmer W, Sengstock K, Sanpera A, Shlyapnikov G V and Lewenstein M 1999 *Phys. Rev. Lett.* **83** 5198
- [20] Denschlag J, Simsarian J E, Feder D L, Clark C W, Collins L A, Cubizolles J, Deng L, Hagley E W, Helmerson K, Reinhardt W P, Rolston S L, Schneider B I and Phillips W D 2000, *Science* **287** 97
- [21] Yulin A V and Skryabin D V 2003 *Phys. Rev. A* **67** 023611
- [22] Scott R G, Martin A M, Fromhold T M, Bujkiewicz S, Sheard F W and Leadbeater M 2003 *Phys. Rev. Lett.* **90** 110404
- [23] Peyrard M and Kruskal M D 1984, *Physica D* **14** 88
- [24] Kevrekidis P G and Weinstein M I 2000 *Physica D* **142** 113
- [25] Ablowitz M J and Musslimani Z H 2003 *Phys. Rev. E* **67** 025601
- [26] Sukhorukov A A and Kivshar Y S 2002 *Phys. Rev. E* **65** 036609
- [27] Feng J and Kneubühl F K 1993 *IEEE J. Quantum Electron.* **29** 590
- [28] Abdullaev F Kh, Baizakov B B, Darmanyan S A, Konotop V V and Salerno M 2001 *Phys. Rev. A* **64** 043606
- [29] Alfimov G L, Konotop V V and Salerno M 2002 *Europhys. Lett.* **58** 7
- [30] Kevrekidis P G, Carretero-Gonzalez R, Theocharis G, Frantzeskakis D J and Malomed B A, *Phys. Rev. A* **68**, 035602
- [31] Kivshar Y S and Campbell D K 1993 *Phys. Rev. E* **48** 3077
- [32] Sukhorukov A A and Kivshar Yu S 2003 *Phys. Rev. Lett.* **91** 113902.
- [33] Kivshar Y S and Luther-Davies B 1998 *Physics Reports* **298** 81

- [34] Bronski J C, Carr L D, Deconinck B and Kutz J N 2001 *Phys. Rev. Lett.* **86** 1402
- [35] Ahufinger V, Sanpera A, Pedri P, Santos L and Lewenstein M 2003 arXiv: cond-mat/0310042.
- [36] The xmds website is located at <http://www.xmds.org/>